

pubs.acs.org/acsaelm Article

# System-Level Network Analysis of a Catechol Component for Redox Bioelectronics

Zhiling Zhao, Si Wu, Eunkyoung Kim, Chen-yu Chen, John R. Rzasa, Xiaowen Shi, William E. Bentley, and Gregory F. Payne\*



Cite This: ACS Appl. Electron. Mater. 2022, 4, 2490-2501



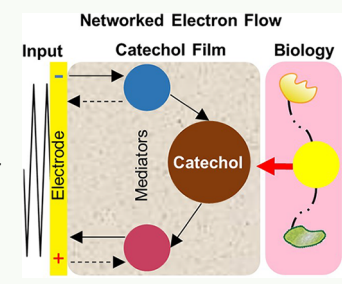
**ACCESS** 

Metrics & More

Article Recommendations

SI Supporting Information

ABSTRACT: Redox is a ubiquitous biological signaling modality that is providing opportunities for bioelectronics. Various experimental studies have demonstrated that catechols offer unique molecular electronic properties for redox-based bioelectronics because catechols can confer redox activity without conductivity. Here, we fabricated a catechol-containing hydrogel film at an electrode surface and characterized this film using dynamic spectroelectrochemical measurements and physics-based modeling (i.e., reaction—diffusion modeling). We show that (i) the flow of electrons through the catechol film involves a redox reaction network; (ii) the redox-state switching of the catechol node is gated by diffusible electron carriers (i.e., mediators) and synchronized to electron transfer at the electrode; and (iii) a physics-based reaction—diffusion model can be abstracted into readily measurable metrics that can be used to characterize the



response characteristics of more complex experimental systems (i.e., systems that cannot be described from first principles). Finally, we performed a simple perturbation analysis to illustrate how theory can guide the selection of metrics capable of detecting interactions between the catechol-coated electrode and bio-relevant nodes of a redox interactome (i.e., metrics that are sensitive to redox network topology). Overall, this work provides a unifying framework to understand catechol-based electrode coatings and suggests how theory can guide the selection of metrics for data-driven analysis in emerging applications in redox bioelectronics.

KEYWORDS: catechols, redox-based bioelectronics, networked electron flow, redox network analysis, mediated electrochemistry, metrics

# **■ INTRODUCTION**

Redox-based bioelectronics is an emerging technology that is fundamentally different from conventional bioelectronics in that it interfaces through biology's redox modality (not biology's ion-based electrical modality). One critical difference is that electrons (not ions) are the charge carriers for the redox modality.<sup>2-4</sup> Because electrons are not soluble, the "flow" of electrons through biology's redox modality generally involves electron transfer reactions between molecules that serve as nodes in a redox reaction network as illustrated by the redox interactome of Scheme 1a.5-8 A second difference is the application space. Conventional ion-based bioelectronics often connects through biology's neuromuscular systems with particular successes involving cardiovascular health: The system-level status can be readily observed (e.g., by an EKG), maintained (e.g., by a pacemaker), and adjusted (e.g., by a defibrillator). In contrast, redox-based bioelectronics offers the opportunity to connect through other biological systems (e.g., the immune system) and targets other applications such as the system-level measurement of oxidative stress<sup>9-14</sup> and the actuation of gene expression (electrogenetics). 15-19

The emergence of redox-based bioelectronics has been driven by various experimental demonstrations each involving individualized approaches to signal analysis. The goal of the work reported here is to provide a generic framework to relate

system-level bioelectronic measurements (e.g., of electrical activities) to the underlying molecular-level phenomena. By analogy to conventional bioelectronics, it is useful to consider how Hodges and Huxley related the measurable electrical activities of the ionic-electrical modality to the underlying molecular-level phenomena for signal generation by nerve cells. Specifically, they used an electrical analogy with the membrane serving as a capacitor, the ion channels as conductors, and the ion pumps as current sources. Critical to their formulation was a voltage-gated conductance. The success of the Hodges and Huxley analysis is that it provided a theory-guided framework to complement bottom-up studies (e.g., of voltage-gated ion channels) and also enabled extension to different biological systems (e.g., from the nervous to the cardiovascular system).

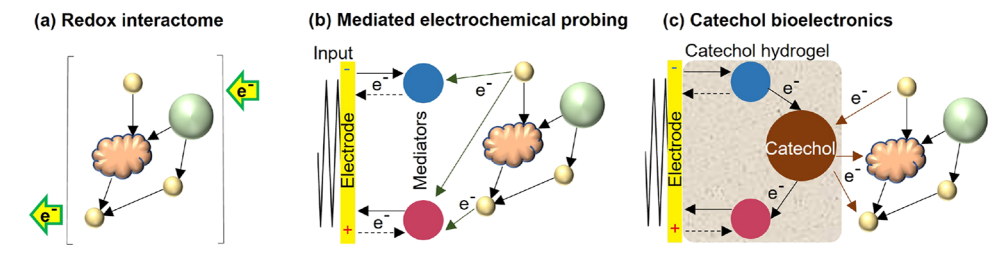
Because the flow of the charge carrier (i.e., the electron) in the redox modality involves a redox reaction network, we propose a network framework (not an electrical analogy) to analyze the relationship between system-level measurements and the underlying molecular phenomena. As illustrated in

Received: February 26, 2022 Accepted: May 4, 2022 Published: May 12, 2022





## Scheme 1. Accessing the Electrical Features of the Redox Modality<sup>a</sup>



"(a) In the redox modality, electrons "flow" through a redox reaction network. (b) Mediated electrochemical probing (MEP) uses mediators and voltage inputs to induce electron flow that evoke output response signals. (c) Catechol is an important molecular electronic component because it serves as a network "hub" capable of exchanging electrons with various biological and electrochemical reductants/oxidants.

Scheme 1a, the molecular nodes of the redox interactome are "linked" through electron transfer reduction/oxidation reactions. Importantly, since an electron transfer reaction switches a node's redox state and since the optical properties of many nodes vary with the redox state, optical measurements have emerged as a convenient source of orthogonal information (i.e., both electrical and optical signals are often measured). <sup>9,20</sup> Thus, a successful framework for analyzing redox networks should be able to explain the observed voltage gating as well as relate both the electrical and optical output signals to the underlying molecular phenomena.

The experimental method used in this study is mediated electrochemical probing (MEP), which is emerging as an important system-level method for redox biology. 4,12,19 Typically for MEP, Scheme 1b shows that diffusible mediators (i.e., nodes) are purposefully added to an experimental system and then an electrode is used to impose tailored voltage inputs that induce electrons to flow through the interactome. When MEP is used for sensing, the mediator and voltage inputs are designed to evoke readily measurable output responses that reveal network topology-dependent features. Two broad goals for MEP sensing are to design mediator/voltage inputs that maximize the information content of the output responses and to analyze these evoked output signals to maximize information extraction. To date, these design and analysis goals have been approached empirically on a case-by-case basis using chemical/biological intuition<sup>9,11</sup> or data-driven statistical analysis. 10,21 Here, we propose a theory-guided framework that can be broadly applied to explain existing results with comparatively simple experimental systems. Ultimately, we envision that this theory-guided framework can be coupled with data-driven analysis to characterize more complex systems (e.g., for network reconstruction of a redox interactome). 22,23

The specific experimental measurements to be analyzed in this study are obtained by electrodes coated with hydrogel containing redox-active catechol moieties. As illustrated in Scheme 1c, catechol-containing hydrogels have emerged as important signal-processing components in redox bioelectronics because they offer unique abilities to bridge redoxbased communication between biology and electronics.<sup>2,24-31</sup> From the biology side, the hydrogel-embedded catechols serve as redox "hubs" capable of interacting with a broad range of interactome nodes (i.e., catechols can exchange electrons with various biological reductants and oxidants). From the electronic device side, the film-embedded catechols can also interact with various electrochemically active mediators that are responsible for shuttling electrons to/from the electrode to generate the electrical output signals (i.e., currents). From a chemistry perspective, these catechol hubs "catalyze" the

directed transfer of electrons from reductants (i.e., "parent" nodes) to oxidants (i.e., "child" nodes).

Here, we employ a reaction—diffusion framework of the underlying physical phenomena to describe the networked flow of electrons through the catechol-based hydrogels. We show that, for simple experimental systems, this framework can characterize how the electrical and optical output signals emerge from the networked flow of electrons and the molecular switching of the various nodes. Further, we illustrate how this framework can be extended to more complex applications (e.g., to characterize topology-dependent signal perturbations) by using theory-informed signal metrics to guide data-driven analysis.

## **■ EXPERIMENTAL SECTION**

**Materials.** Chitosan, catechol, Ru(NH<sub>3</sub>) $_6$ Cl<sub>3</sub>, 1,1-ferrocenedimethanol, and ascorbate were purchased from Sigma-Aldrich. All reagents were used as received without further purification. All solutions were prepared using Millipore water (>18 M $\Omega$ ). The solutions of mediators with/without ascorbate were prepared in 0.1 M phosphate buffer (pH 7.0).

Instrumentation. The spectroelectrochemical cell consisted of a screen-printed gold transparent (4 mm diameter; from Metrohm, Spain) working electrode, a AglAgCl reference electrode, and a counter electrode made of 0.3 mm platinum wire. A potentiostat (CHI 420A, CH Instruments) was used for the electrofabrication of catechol films and all the electrochemical measurements. A UV—vis spectrophotometer (Evolution 60, Thermo Scientific) was used for the spectro-measurements, which was carried out simultaneously with the electrochemical measurements.

**Spectroelectrochemical Probing.** The catechol films were fabricated on the gold transparent electrode using a two-step method (see Scheme S1 of the Supporting Information for detailed information). The catechol-coated (or control chitosan-coated) gold electrode was used in the spectroelectrochemical cell as the working electrode. The solution of mediators (0.1 mM ferrocene dimethanol and 0.1 mM  $Ru(NH_3)_6Cl_3$ ) was degassed with with  $N_2$  for 20 min before the measurements.

# ■ RESULTS AND DISCUSSION

**Catechol Hydrogel Films.** The catechol hydrogel films (several hundred micrometers thick when wet) were electrofabricated in two simple steps as previously reported (see the Supporting Information for further description of electrofabrication).<sup>32–34</sup> There are two important features of the catechol hydrogel films. First, the hydrogel remains permeable and allows small molecules (e.g., mediators) to diffuse between the external solution and the electrode surface. Second, the grafted catechols confer redox activity to the films as these catechols can be repeatedly switched between their oxidized and reduced states; however, these films are non-conducting

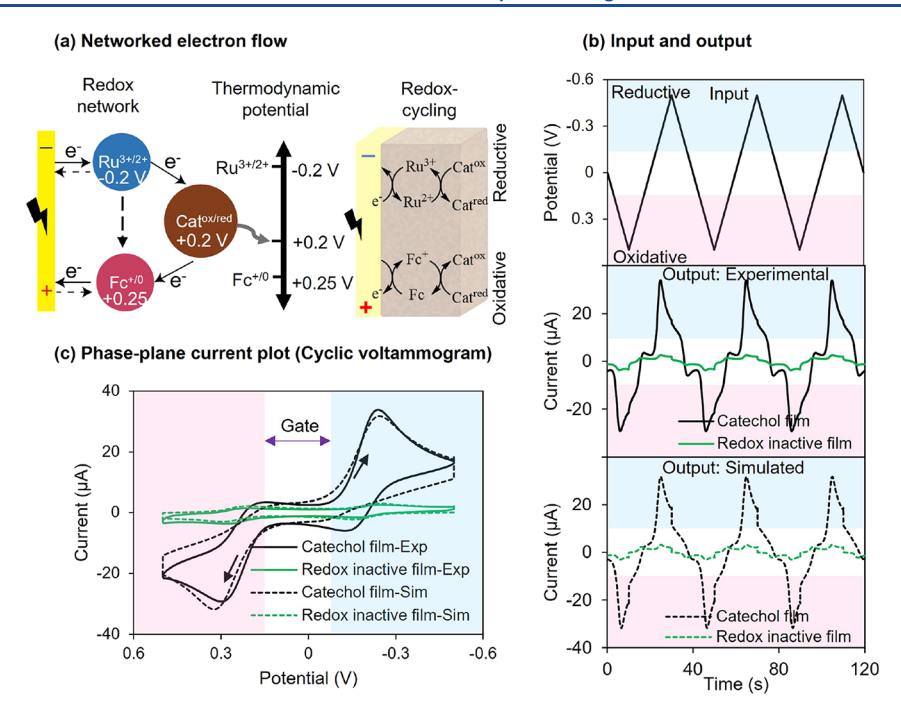


Figure 1. Networked flow of electrons through the catechol hydrogel film. (a) Network description shows the mediated flow of electrons through three nodes  $(Fc^{+/0}, Ru^{3+/2+}, and Cat^{ox/red})$ , while a chemistry description shows that electron transfer involves two redox-cycling mechanisms. (b) Output current time-series curves are used to characterize the flow of electrons; simulations using a network model recapitulate key experimental observations. (c) Phase-plane plots of the input potential and output current responses show that gating is due to the mediators' redox potential (CV plot for the first cycle of the three cycle time-series). Experimental data were generated using a mediator solution containing both ferrocene dimethanol (0.1 mM) and  $Ru(NH_3)_6Cl_3$  (0.1 mM) in phosphate buffer (0.1 M, pH 7.0) and a scan rate of 50 mV s<sup>-1</sup>.

and the direct electron exchange with the electrode is negligible (see Figure S1 of the Supporting Information). Presumably, the catechols that are immobilized in the film are too far from the electrode surface to allow direct electron transfer. Further, the grafted catechols are redox-active because they have two stable states (oxidized and reduced), but presumably, these grafted catechols do not form an extended conjugation system that would allow the flow of electrons in response to an applied electric field (i.e., the grafted catechol polymers are not conducting polymers). Rather, electron transfer to/from the grafted catechols requires diffusible mediators.

Electron Flow in the Catechol Redox Network. As illustrated in Figure 1a, the flow of electrons through the catechol film results from a mediator-based redox reaction network (and not the flow through a conducting material). Here, we used the common electrochemical mediator pair of Ru(NH<sub>3</sub>)<sub>6</sub>Cl<sub>3</sub> (Ru<sup>3+</sup>) and ferrocene dimethanol (Fc), and Figure 1a shows this directed three-node (Catox/red, Ru3+/2+, and Fc<sup>+/0</sup>) redox network. The Ru<sup>3+</sup> mediator has a reducing redox potential ( $E^0 = -0.2 \text{ V}$  vs AglAgCl) and can reversibly exchange electrons with the electrode with the direction and rate of electron transfer being controlled by the applied electrode voltage. Both forms of this mediator (oxidized or reduced) can diffuse into the film, but the reduced form (Ru<sup>2+</sup>) can donate electrons to grafted catechol moieties ( $E^0 = +0.2 \text{ V}$ vs AglAgCl), thus converting the oxidized quinone state (Cat<sup>ox</sup>) into the reduced catechol state (Cat<sup>red</sup>). Thermodynamically, the interaction between these two nodes is constrained such that electrons flow from the Ru3+/2+ node to the Cat<sup>ox/red</sup> node (but not in the reverse direction). Chemically, this mediated electron transfer involves a reductive redox-cycling mechanism illustrated in Figure 1a. Similarly, the

Fc<sup>0</sup> mediator, which has an oxidizing redox potential ( $E^0$  = +0.25 V vs AglAgCl), can reversibly exchange electrons with the electrode with the direction and rate of electron transfer being controlled by the applied electrode voltage. Both forms can diffuse into the film, but the oxidized form (Fc<sup>+</sup>) can accept electrons from the catechol node in a thermodynamically constrained oxidative redox-cycling mechanism also illustrated in Figure 1a.

In contrast to conventional electronics where current flow depends on the materials' conducting or semi-conducting properties, the flow of electrons through the catechol film is controlled by the topology of the redox network and the "weights" (i.e., reaction rates) for the node-node interactions. To provide a physically realistic description of electron flow through this network, we used commercially available finite element analysis software (COMSOL Multiphysics 5.6) to account for three phenomena: the electrochemical reactions associated with electron transfer between the electrode and the mediators ( $Ru^{3+/2+}$  and  $Fc^{+/0}$ ), the diffusion of the mediators to/from the electrode surface, and the electron transfer redox reactions between the mediators and the immobilized catechols (details provided in Figure S2 and Table S1). This "minimal" electrochemical reaction-diffusion model aims to provide a theory-guided framework to discern topologydependent dynamic behavior, enable perturbation analysis, and allow extension to more complex data-driven analysis (i.e., to reverse engineer an unknown redox network). While we do not aim to create a digital replica in the present contribution, we expect that this model could be parameterized for extension to specific applications.

Experimentally, the electron flow through this redox network was characterized by measuring the output current when an oscillating voltage was applied. As shown in Figure 1b, a

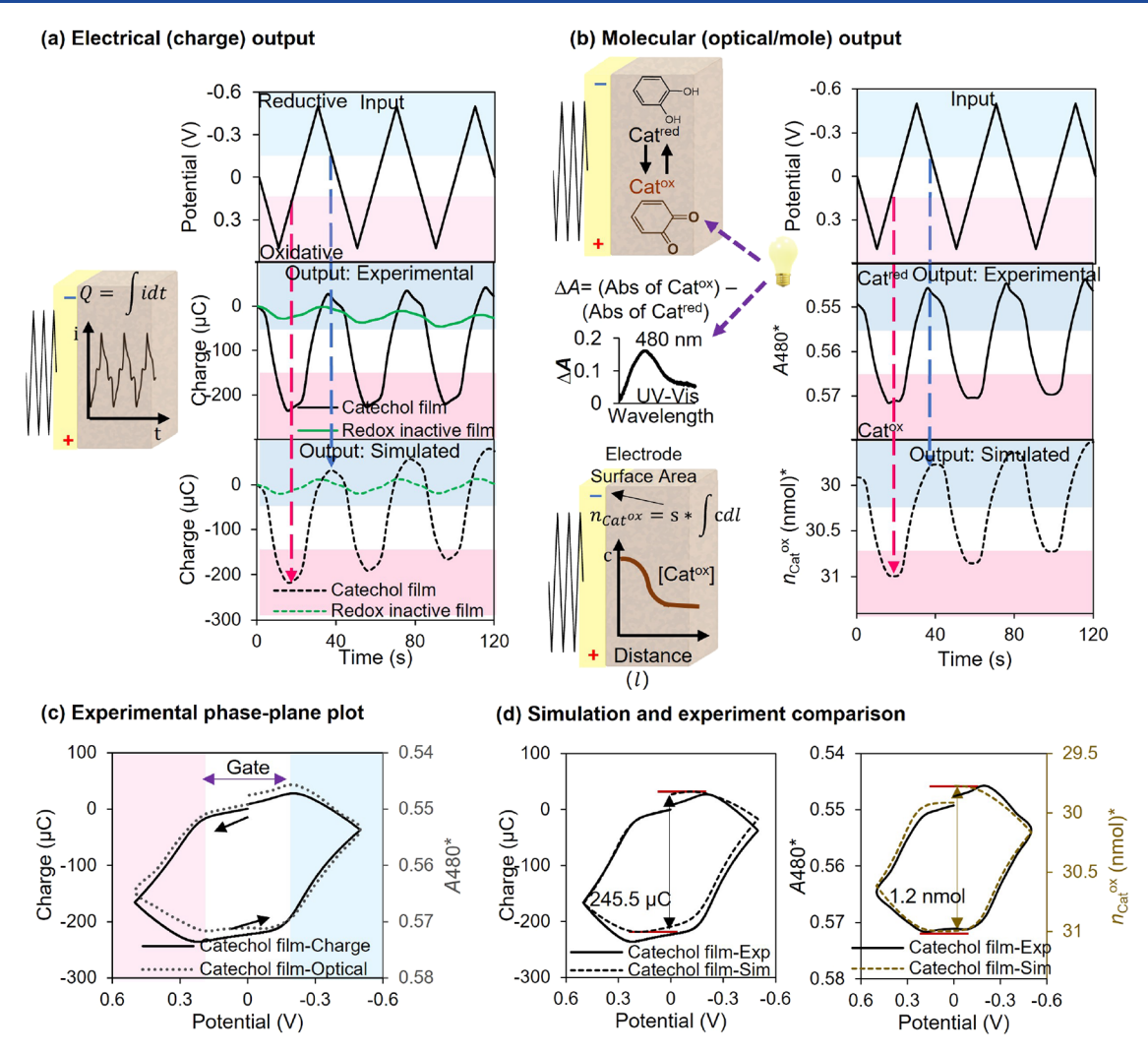


Figure 2. Molecular switching of the catechol film/node. (a) Comparison of the electrical charge time-series output  $(Q = \int idt)$  from spectroelectrochemical measurement and simulation. (b) Comparison of the molecular time-series output from spectroelectrochemical measurement (optical absorbance at a wavelength of 480 nm) and simulation proxy  $(n_{\text{Cat}}^{\text{ox}})$  obtained by integration of the concentration of  $\text{Cat}^{\text{ox}}$ ). (c) Phase-plane plot shows that the molecular switching of catechol was synchronized with electron flow (the first cycle of the three-cycle time-series). (d) Simulated phase-plane plots of charge and molecular responses are similar to experimental measurements. (\* axes are inverted to facilitate comparison).

triangular wave is imposed, varying between -0.5 and 0.5 V with a cycle time of 40 s at a scan rate of 50 mV s<sup>-1</sup>. The data was measured in mediator solution with electrodes that were coated with either a catechol hydrogel or a control redoxinactive chitosan hydrogel.<sup>35</sup> When the input voltage is cycled into the oxidative region (positive voltages), the output shows that anodic (negative) currents are generated. Similarly, when the input voltage is cycled into the reductive region (negative voltages), cathodic currents are generated. Both experimental and simulated output responses show considerable amplification of currents for the catechol hydrogel, which is consistent with the mediator redox-cycling mechanisms in Figure 1a.

The input—output data can also be analyzed using phase-plane analysis, and such a plot for current and voltage is known as a cyclic voltammogram (CV). Visually, the CV curves of Figure 1c for the experimental results are reasonably similar to those simulated by the electrochemical reaction—diffusion model. Both the simulated and experimental curves show the commonly observed current amplifications for the catechol hydrogel (vs redox-inactive control hydrogel) in the  $Ru^{3+}$  reduction (less than -0.15~V) and  $Fc^0$  oxidation (>0.2 V)

regions.<sup>36</sup> Also, both plots in Figure 1c illustrate the mediator gating of the currents: Low and nearly constant currents are observed in the central voltage region where the mediators are "inactive", while currents are allowed to flow in voltage regions near the mediator's  $E^0$  value.

In addition to replicating the distinctive amplifications and gating associated with the networked flow of electrons through the catechol hydrogel, the model can also provide insights of the spatiotemporally changing concentrations of the mobile charge carriers (i.e., the mediators), which is difficult/ impossible to observe experimentally. As detailed in the Supporting Information (i.e., Figure S3), results from this model yield three interesting insights. First, there are no significant interactions between the  $Ru^{3+/2+}$  and  $Fc^{+/0}$ mediators. The dotted line in Figure 1a suggests the possibility that the reduced Ru<sup>2+</sup> could donate electrons to the oxidized Fc<sup>+</sup>, but simulations indicate that the active states of these mediators (i.e., Ru<sup>2+</sup> and Fc<sup>+</sup>) do not co-exist in the same place at the same time (Figure S3d). Second, for the case of the redox-inactive control film, the mediators' active redox states generated at the electrode (i.e., Fc<sup>+</sup> and Ru<sup>2+</sup>) penetrate

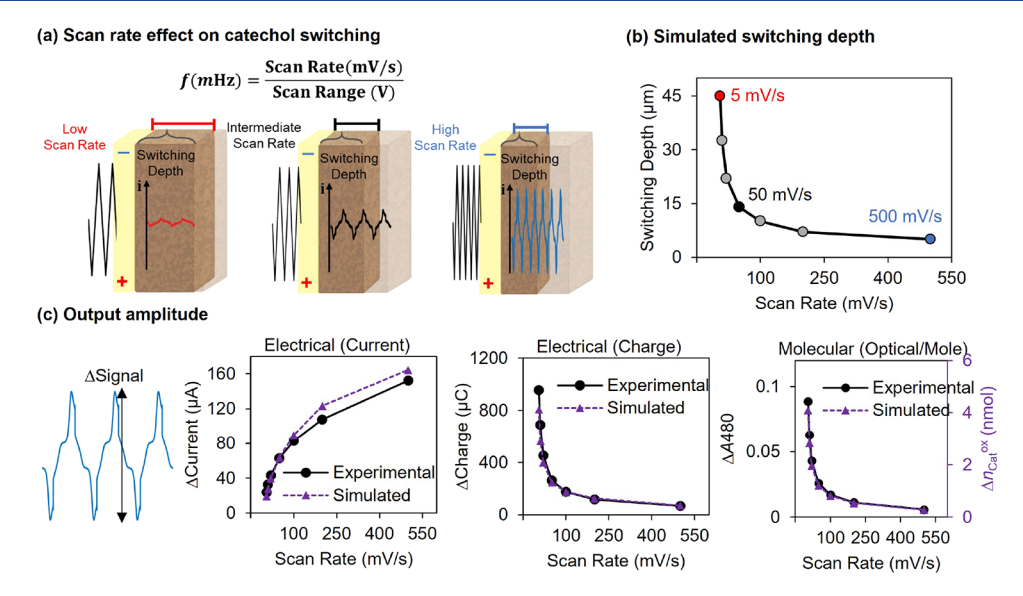


**Figure 3.** Dynamic analysis of signals. (a) Schematic illustrating how the scan rate (or frequency) is expected to affect the molecular switching depth and current signal. (b) Simulated catechol switching depth. (c) Frequency-dependent signal characteristic (amplitude) of the catechol film and comparison to simulations (the simulated proxy for the molecular signal is  $n_{\text{Cat}}^{\text{co}}$ ).

approximately 180  $\mu$ m into this redox-inactive control film (Figure S3e). Third, for the case of the catechol film, the active redox states of these mediators penetrate only about 15  $\mu$ m into the film (Figure S3e), and this narrower penetration is due to the redox-cycling reactions (Figure 1a) that rapidly "quench" these mediators' active redox states.

In summary, the electron flow through the catechol film is networked while the time-series current response (i-t) and phase-plane CV (i-V) plots can characterize the underlying molecular phenomena of mediator diffusion and electron-transfer reactions.

Molecular Switching of the Catechol Node. In addition to current (i), a second electrical output response is charge (Q =  $\int idt$ ), and previous studies indicate that Q can be related to the molecular switching of the catechol node.<sup>20</sup> We performed this mathematical integration for both the experimental and simulated current output data from Figure 1b, and Figure 2a shows that Q oscillates over time. In comparison, the experiment and simulation show a co-localization of the peaks for oxidative charge (red dotted line) and reductive charge (blue dotted line). Moreover, both experiment and simulation show that the catechol film's charge output oscillates with a large amplitude (compared to the redoxinactive control film) indicating significant accumulation of electrons in the catechol film during the reductive segment and significant depletion of electrons from the film during the oxidative segment. This accumulation and depletion of electrons are consistent with the molecular switching of the catechol node's redox state.

The molecular switching of the catechol node can be observed experimentally using optical measurements since the catechol's oxidized state ( $\operatorname{Cat}^{\operatorname{ox}}$ ) has a darker color and larger absorbance at 480 nm than its reduced state ( $\operatorname{Cat}^{\operatorname{red}}$ ).<sup>20</sup> The middle plot in Figure 2b shows an oscillating optical output ( $A_{480}$ ) for the three-cycle time-series from the same spectroelectrochemical measurements of Figure 2a. To facilitate visual comparison of the plots of Q (Figure 2a) and  $A_{480}$  (Figure 2b), we inverted the scale for  $A_{480}$  so the maximal  $\operatorname{Cat}^{\operatorname{ox}}$  values appear at the bottom of the plot (i.e., the oxidation region). This comparison illustrates that the outputs

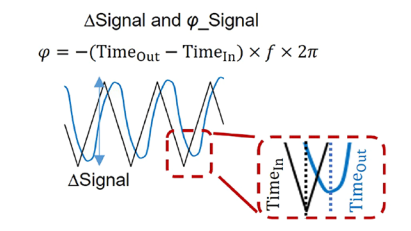
Q and  $A_{480}$  are in-phase with each other (i.e., synchronized) and out of phase with the input voltage.

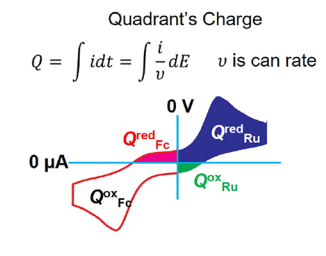
The next goal was to create a computable proxy for the experimental observable  $(A_{480})$  associated with molecular switching of the catechol node's redox state. The molecular switching of catechol's redox state can be simulated since the electrochemical reaction-diffusion model yields information of how the concentrations of Catox and Catred vary as a function of position and time (the comparison with a redox-inactive control film is shown in Figure S4, and simulated concentration profiles with the redox-active catechol film are shown in Figure S5). As illustrated by the schematic at the bottom of Figure 2b, we integrated the concentration of Catox as a function of position to determine the total amount of the oxidized state  $(n_{Cat}^{ox})$ . The lower plot in Figure 2b shows the three-cycle time-series of this simulated proxy for the molecular output  $(n_{\text{Cat}}^{\text{ox}})$ . Again, to facilitate visual comparison, we inverted the scale for  $n_{\text{Cat}}^{\text{ox}}$  such that the lower (red) region of the plot is more oxidative. Figure 2b shows that the oscillations for the simulated proxy (i.e.,  $n_{\text{Cat}}^{\text{ox}}$ ) and experimental observable (i.e.,  $A_{480}$ ) for redox state switching are in-phase with each other and also in-phase (i.e., synchronized) with the charge output Q in Figure 2a.

To further investigate the relationship between the number of electrons flowing into the hydrogel (as measured by Q) and the molecular switching of the catechol node (as measured by  $A_{480}$ ), we show these experimental results in the same phaseplane plot in Figure 2c. The first observation in Figure 2c is the similarity in shapes of these two phase-plane plots. This similarity is consistent with the synchronization of these two outputs observed in time-series plots and also consistent with previously reported spectroelectrochemical correlations between optically observed switching and electrically observed  $Q^{20}$ . The second observation in Figure 2c is that the majority of the change in Q and  $A_{480}$  occurs in the Ru<sup>3+</sup>-reduction (less than -0.15 V) and Fc<sup>0</sup>-oxidation (>0.2 V) regions, consistent with the roles of these mediators to gate the molecular switching of the catechol node's redox state.

The comparison between experiment and simulations for the phase-plane plots for charge (Q) and molecular switching is

#### (a) Signal metrics





#### (b) Correlation between experimental and simulated metrics

|                | ΔCurrent | ∆Charge | $\Delta A_{480}$ $(\Delta n_{\text{Cat}}^{\text{ox}})$ | $\phi$ _Current | $\phi$ _Charge | $\phi_A_{480}$ ( $\Delta n_{Cat}^{ox}$ ) | Q <sup>ox</sup> Fc | Q <sup>red</sup> Fc | Q <sup>red</sup> <sub>Ru</sub> | Q <sup>ox</sup> Ru |
|----------------|----------|---------|--|-----------------|----------------|--|--------------------|---------------------|--------------------------------|--------------------|
| R <sup>2</sup> | 0.996    | 0.999   | 1.000  | 0.988           | 0.028          | 0.166                                    | 0.988              | 0.281               | 0.975                          | 0.550              |
| Р              | 3.1E-7   | 3.1E-8  | 6.1E-10  | 5.5E-6          | 0.72           | 0.36                                     | 5E-6               | 0.22                | 3.3E-5                         | 0.06               |
| slope          | 1.167    | 0.808   | N/A  | 2.211           | -0.655         | 0.038                                    | 0.771              | 0.062               | 0.886                          | -0.038             |

#### (c) Experimental metrics plotted versus simulations

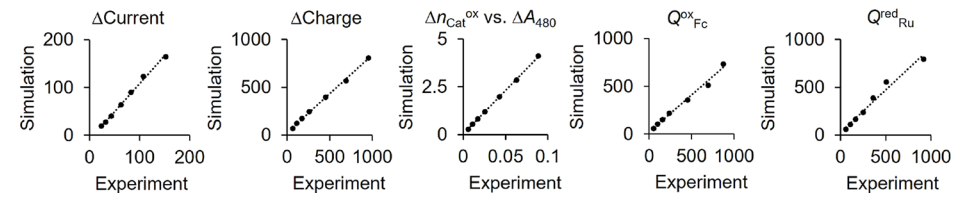


Figure 4. Proposed metrics. (a) Schematic illustrating signal metrics extracted from time-series data and phase-plane CV plot. (b) Correlation between experimental and simulated metrics identified five potentially reliable metrics. (c) Comparison of experimental and simulated metrics.

shown in Figure 2d. The leftmost plot shows good qualitative and quantitative agreement for Q between experiment and simulation. The rightmost plot shows good qualitative agreement between the experimentally observed  $A_{480}$  and its simulated proxy  $n_{\text{Cat}}^{\text{ox}}$ .

These simulations allow a quantitative comparison of the electron flow through the network and molecular switching using amplitudes of the oscillating outputs. Specifically, the simulated amplitudes of the oscillating charge  $\Delta Q$  (245.5  $\mu C$ ) and molecular switching  $\Delta n_{\text{Cat}}^{\text{ox}}$  (1.2 nmol) can be compared to a theoretical value, assuming that all the electrons transferred at the electrode pass through the catechol node and two electrons are required to switch each catechol's redox state<sup>37</sup> (1.272 nmol =  $\frac{\Delta \hat{Q}}{zF}$ ,  $\Delta Q$  = 245.5  $\mu C$  , z = 2, and F = 96,485 C/mol). This comparison suggests that 94% (= 1.2/ 1.272) of the electrons transferred at the electrode pass through the catechol node: They are accumulated and stored during the reductive segment and depleted during the oxidative segment. The remaining 6% of the electron transfer is presumably due to the reversible electron exchange between the mediators and electrode. Overall, the results in Figure 2 indicate that the molecular switching of the catechol node is synchronized with the electron transfer at the electrode, indicating that the mediators gate the flow of electrons to the Cat<sup>ox/red</sup>, consistent with the network of Figure 1a.

**Dynamic Analysis.** The experimental results and simulations in Figures 1 and 2 support the conclusions that (i) the flow of electrons through the catechol film occurs through a three-node redox reaction network, and (ii) the catechol node undergoes repeated molecular switching of its redox state. A more rigorous dynamic analysis considers the frequency dependence of these time-series electrical and molecular features. The schematic in Figure 3a illustrates the intuitive

expectations that increasing the scan rate (or frequency) of the imposed voltage should provide less time in each cycle for the mediators to diffuse and the catechol moieties to be switched by redox cycling; thus, the switching depth should decrease with increasing scan rate. To quantify this expectation, we performed simulations at seven scan rates (5–500 mV s<sup>-1</sup>), examined the concentration profile for Cat<sup>ox</sup> at the time near the maximum oxidation of this Cat<sup>ox/red</sup> node, and estimated the switching depth from this gradient. The switching depth is summarized in Figure 3b and shows a decrease with increasing scan rate.

Next, we compared the dynamic responses of signals from experimental spectroelectrochemical measurements with simulations (further comparisons of responses are shown in Figures S6 and S7). Figure 3c summarizes the frequency (f) dependence of three signals: the current (i), charge (Q), and catechol film's redox state (observable  $A_{480}$  or computable proxy  $n_{\text{Cat}}^{\text{ox}}$ ). As noted, i reflects the flow of electrons through the catechol film while Q and  $A_{480}$  (or  $n_{Cat}^{ox}$ ) are the electrical and molecular features related to switching of the Catox/red node. As illustrated, we defined the signals' amplitude ( $\Delta$ Signal) as the difference in peak (maximum and minimum) values. [As discussed in Figure S8 of the Supporting Information, a phase difference  $\varphi$  can also be defined for each of these signals, but as discussed below, these phase differences did not provide useful information. Figure 3c shows both experimental results for  $\Delta$ Signal and corresponding simulations. The frequency analysis shows that, at low scan rate, the *i* has a small amplitude ( $\Delta$ Current), and this amplitude increases with increasing scan rate; at low scan rate, the amplitude of Q ( $\Delta$ Charge) is large and decreases with increasing scan rate, and similar to the dynamic response of Q, the absorbance  $(A_{480})$  and its computable proxy  $n_{Cat}^{ox}$  have

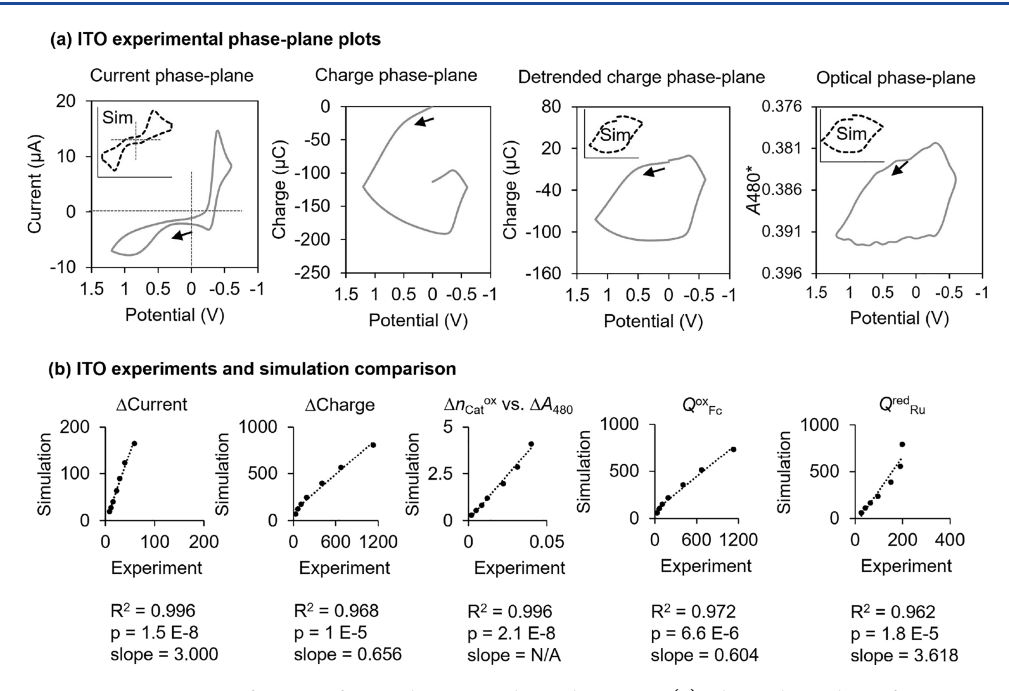


Figure 5. Characterizing outputs in terms of metrics for an alternative electrode system. (a) Phase-plane plots of responses measured for a less electrocatalytically active ITO electrode, while insets show simulations of a minimal model (dashed curves, reproduced from Figures 1c and 2d). (b) Correlation between ITO experiments and simulated metrics shows that, despite large quantitative differences (slopes deviate from 1.0), there remains good statistical agreement between experiment and simulation for the five reliable metrics ( $R^2 > 0.95$  and P < 0.05).

high amplitude at low scan rates and this amplitude decreases with increasing scan rate. This frequency analysis further illustrates that a minimal model captures the essential physics of the mediated flow of electrons and molecular switching of the catechol-based hydrogel film for this simple, well-behaved mediator electrode system.

Abstracting Analysis in Terms of Measurable Signal Metrics. The above results illustrate how the mediated flow of electrons and molecular switching of a catechol film can be described by a physics-based redox reaction network model. Our long-term goal is to extend this theory-guided analysis of mediated electrochemical probing (MEP) to more complex or ill-defined situations that do not lend themselves to a first-principles modeling approach (e.g., to use MEP for the reconstruction of an unknown biological redox reaction network). We envision that a first-principles theoretical framework can be abstracted in terms of readily measurable signal metrics<sup>22</sup> that can be broadly applied to reveal characteristic signatures of such a complex redox network.

The above results suggest that MEP-based signals can be quantified in terms of metrics obtained either from time-series or phase-plane analysis. As illustrated in Figure 4a, time-series data yields amplitude and phase shift metrics for the two electrical outputs ( $\Delta$ Current,  $\Delta$ Charge,  $\varphi$  Current, and  $\varphi$  Charge) and the outputs associated with molecular switching (either the experimental observables  $\Delta A_{480}$  and  $\varphi\_A_{480}$  or the simulated proxies  $\Delta n_{\text{Cat}}^{\text{ox}}$  and  $\varphi\_n_{\text{Cat}}^{\text{ox}}$ ). Further, Figure 4a suggests metrics from phase-plane CV analysis for charge (Q) associated with the oxidation and reduction of each mediator (note: these metrics are operationally labeled in terms of the mediator electrochemical reaction that is expected to be the dominant contributor to the signal in that region). For probing with the two Fc and Ru3+ mediators, four quadrants are shown (i.e.,  $Q^{\text{ox}}_{F\sigma}$   $Q^{\text{red}}_{F\sigma}$   $Q^{\text{ox}}_{Rw}$  and  $Q^{\text{red}}_{Ru}$ ). 38 Possibly, additional metrics could be obtained from phaseplane analysis for charge (Q) or optical (Abs) responses;

however, we are unaware of such metrics. Further, we should note that, if non-oscillatory voltage inputs are imposed (e.g., voltage steps or pulses), then alternative metrics could be defined for transient responses (e.g., signal decay rates): Since our focus here is oscillatory voltage inputs and steady output responses, these transient response metrics are not considered. Overall, the time-series and phase-plane analyses suggest 10 possible signal metrics in Figure 4b that could be used to quantify output responses.

We calculated these 10 metrics from experimental and simulation data for the dynamic analysis study (some of these values are already displayed in Figure 3), and we then performed a statistical comparison to determine which metrics could be well simulated from the theory-guided model. Specifically, we performed linear regression analysis (R version 4.0.2) between the simulated and experimentally observed metrics. Figure 4b shows the linear regression slope coefficient and  $R^2$  and p values for each of these metrics (note: a parameter-optimized digital replica of an errorless experimental system should yield  $R^2$  and slope values near 1.0 and a low p value). According to Figure 4b, five metrics ( $\Delta$ Current,  $\Delta$ Charge,  $\Delta A_{480}$  or  $\Delta n_{\text{Cat}}^{\text{ox}}$ ,  $Q_{\text{Fc}}^{\text{ox}}$  and  $Q_{\text{Ru}}^{\text{red}}$  showed good agreement between experiment and theory (typically  $R^2 > 0.95$ and p < 0.05), while five metrics ( $\varphi$ \_Current,  $\varphi$ \_Charge,  $\varphi_{A_{480}}$  or  $\varphi_{R_{at}}^{ox}$ ,  $Q_{Fc}^{red}$  and  $Q_{Ru}^{ox}$  showed less agreement. Interestingly, these latter metrics were also not suggested to be useful from previous experimental studies,<sup>39</sup> often because of large experimental errors. Figure 4c shows a plot of experimental and simulated values for each of the five "reliable" metrics that showed good agreement between theory and experiment.

Using Metrics to Characterize an Alternative Electrochemical System. The goal of the minimal network model is to provide a theoretical framework that can be abstracted to allow extrapolation to different, more complex situations. The minimal modeling approach considers output responses in

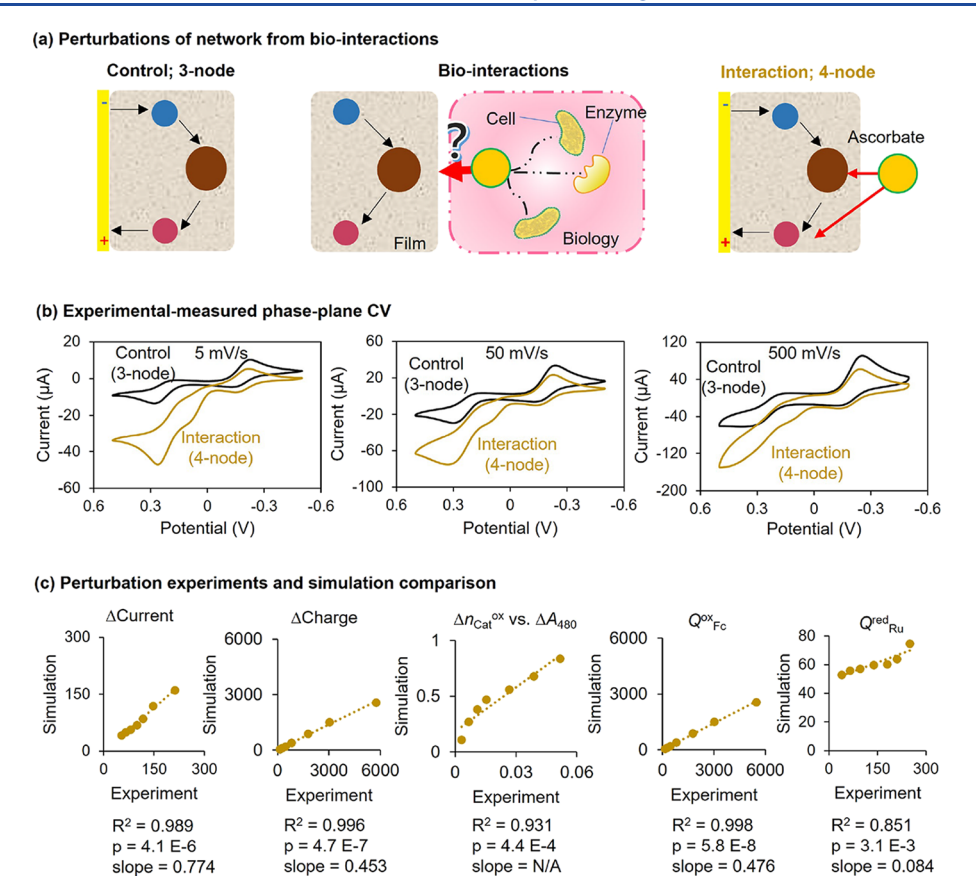


**Figure 6.** Using metrics to characterize bio-relevant redox interactions with the catechol film. (a) Schematic illustrates that biologically relevant redox nodes (e.g., the bio-reductant ascorbate) can interact with the catechol film. (b) Interactions with the ascorbate (the fourth node) affect the shape of experimentally measured phase-plane CV (note the different *y*-axis scales). (c) Correlations between simulation and experiment for the five reliable metrics with the four-node network.

terms of the "primary" physical phenomena of the mediator:diffusion, reactions at the electrode, and reactions with the catechol node. The model neglects "secondary" phenomena such as electrode-specific behaviors, electrode fouling, mediator chelation, or mediator ligand exchange. The goal is to have a theory-driven model to identify readily measurable metrics that can be broadly extended to more complex situations (e.g., to reconstruct an unknown redox interactome).

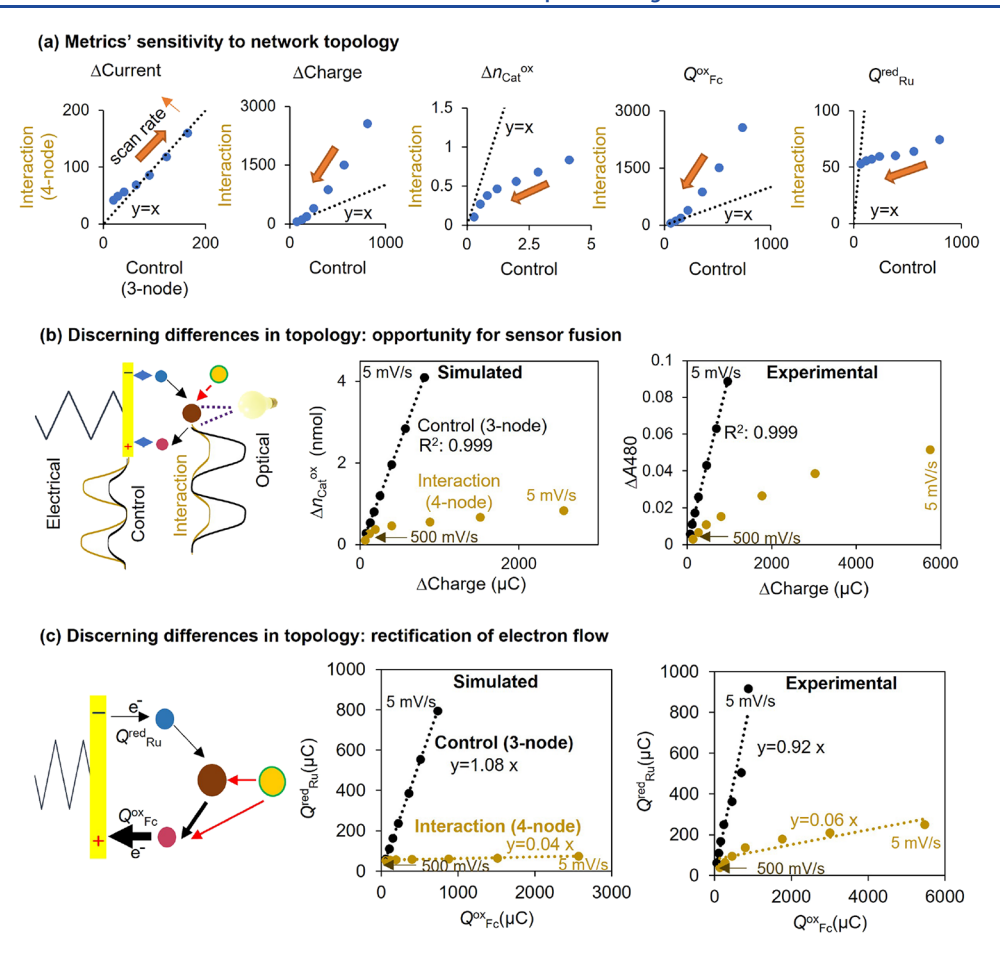
One example is to extend the minimal model to a less idealized electrode system. Here, we used previously reported dynamic spectroelectrochemical measurements from experiments with a transparent indium tin oxide (ITO) electrode that was coated with a similar polysaccharide-catechol hydrogel film and probed using the same Fc and Ru<sup>3+</sup> mediators.<sup>2</sup> Because ITO has a lower electrocatalytic activity than gold,  $^{40}$ experiments were performed using an extended voltage range that resulted in a trend in the time-series data toward increasingly oxidative Q. The experimental Q-t time-series data was detrended using standard methods (i.e., the "detrending" function in the Signal Processing Toolbox of MATLAB), as described in Figure S9 of the Supporting Information. For simulations, we used the same minimal model without parameter optimization. The goal of this example is to test whether theory-guided metrics can be extrapolated to reliably describe essential features of output responses.

Figure 5a shows experimentally observed phase-plane plots with the catechol film-coated ITO electrode, while simulations are generally shown as dashed curves (reproduced from

Figures 1c and 2d). The first phase-plane plot in Figure 5a is the CV curve, and there is general agreement between experiment and simulation in the CV shapes. The second phase-plane plot illustrates the unsteady response of Q, while the third plot illustrates that a detrending of the Q-t curve leads to better agreement between the shapes of the experimental and simulated curves. The final phase-plane plot in Figure 5a shows the molecular response as measured from the optical absorbance  $(A_{480})$  or simulated by its proxy  $n_{\text{Cat}}^{\text{ox}}$ . Overall, these phase-plane plots show general agreement between simulations and experiment, although there are significant quantitative deviations for this less idealized electrode system.

Using the five reliable metrics identified in Figure 4b, we performed a statistical comparison between simulations and the previously reported dynamic spectroelectrochemical experiments. The plots and statistical analysis in Figure 5b show two broad observations. First, there is a strong correlation between simulation and experiment for these five metrics as measured by the statistical parameters (i.e.,  $R^2 > 0.95$  and p < 0.05). Second, despite this statistical agreement, there are significant quantitative differences between experiment and simulation (i.e., the slope values deviate significantly from 1). These observations support the use of a minimal model to identify theory-based extrapolatable metrics.

Using Metrics to Characterize Different Redox Networks. As noted, an important application of catechol-based films is redox-based bioelectronics where the catechol node



**Figure 7.** Topology-dependent metrics for perturbation analysis. (a) Identifying topology-sensitive signal metrics by comparing simulated responses for the three- and four-node networks (orange arrows show the direction of increasing scan rate; y = x line indicates topology independence). Differences in network topology can also be detected (b) by coupling orthogonal electrical and molecular measurements and (c) by characterizing the rectification of electron flow.

facilitates redox-based communication between electronics and biology (e.g., to sense and actuate biology). A1-43 Specifically, Figure 6a illustrates that the catechol node can exchange electrons with biological oxidants/reductants and thus can interface into enzymatic A4,45 or cellular Redox networks. From a network analysis perspective, these biological interactions add nodes to the three-node (mediators plus catechol) network. From an electronics perspective, these added network interactions should be detectable based on their perturbations to the flow of electrons and molecular switching of the catechol film.

To demonstrate a simple perturbation, we considered the addition of the common physiological reductant ascorbate, <sup>48,49</sup> and the right-most scheme in Figure 6a depicts this perturbation as the addition of a single (yellow) node with two directed interactions. Experimentally, Figure 6b compares the phase-plane CV plot for a catechol film-coated gold electrode in the absence of ascorbate (i.e., the non-interacting three-node network) and in the presence of 7.5 mM ascorbate (i.e., the interacting four-node network). These experimental results show that the addition of ascorbate perturbs the phase-plane CV by amplifying the current in the oxidizing voltage region (>0 V) and attenuating the current in the reducing voltage region (<0 V).

For simulations, we used the directed four-node network depicted in Figure 6a and assumed that all node-node interactions could be described by the same rate constants (i.e.,

a minimal model that focuses on network topology). This simplifying network depiction also ignores the direct electron transfer of ascorbate with the electrode: The electrochemical oxidation of ascorbate while possible<sup>50</sup> is sluggish and irreversible, and we reasoned that the Fc+ mediator and grafted quinone (Catox) would preferentially oxidize the ascorbate diffusing into the film from the bulk solution. 10,44 Such simplifying assumptions are commonly required when extending dynamic kinetic models to system-level network analysis. S1 The comparison between simulation and experiment for this four-node network is summarized in Figure 6c (see Figure S10 for more details of this comparison). This comparison shows that the five metrics that had previously been found to be reliable ( $\Delta$ Current,  $\Delta$ Charge,  $\Delta A_{480}$  or  $\Delta n_{\text{Cat}}^{\text{ox}}$ ,  $Q_{\text{Fc}}^{\text{ox}}$  and  $Q_{\text{Ru}}^{\text{red}}$  were also reliable in terms of extending analysis from a three- to a four-node network. In particular, the statistical parameters of  $R^2$  and p show a good linear correlation for most of these five metrics, despite the quantitative discrepancies in predications (i.e., the slope values are significantly different from 1.0).

Identifying Topology-Dependent Metrics for Perturbation Analysis. While the above examples illustrate that the output responses can be abstracted in terms of five reliable signal metrics, these metrics are only useful if they provide valuable system-level insights. Since one long-term goal of mediated electrochemical probing (MEP) is to "reconstruct" an unknown biological redox reaction network, a metric would

be useful if it was sensitive to this interactome's network topology. Thus, we examined how the five reliable metrics were perturbed by interactions of the catechol film with an external node. Specifically, we performed a perturbation analysis to identify how the addition of an "ascorbate" node perturbed the output metrics compared to those from the three-node, Cat<sup>ox/red</sup>-Ru<sup>3+/2+</sup>-Fc<sup>+/0</sup>, network (i.e., we compared the four- and three-node networks). Figure 7a compares simulated metric values obtained from dynamic analysis for the four-node (y axis) vs three-node (x axis) networks for each of the five reliable metrics. The dotted lines (y = x) in these plots correspond to a topology-independent response. The results in Figure 7a indicate that four of these metrics are expected to be sensitive to topology ( $\Delta$ Charge,  $\Delta A_{480}$  or  $\Delta n_{\text{Cat}}^{\text{ox}}$ ,  $Q^{\text{ox}}_{\text{Fe}}$  and Q<sup>red</sup><sub>Ru</sub>), while one metric has a weaker topology dependence ( $\Delta$ Current). While these four sensitive metrics may be useful individually, combinations of metrics often offer greater discriminating abilities through multivariant and data-driven machine learning analysis. <sup>21,22,51–53</sup>

One example of combining metrics involves sensor fusion where information from orthogonal electrical measurements (i and Q) and optical measurements  $(A_{480})$  is combined to couple information of electron flow and molecular switching of the catechol film. These orthogonal spectroelectrochemical measurements collect high dimensional data, from which we extract representative values (i.e., metrics) that could be further used for data-driven (e.g., principal component) analysis to characterize complex redox network systems. Figure 7a illustrates that  $\Delta Q$  and  $\Delta n_{\rm Cat}^{\rm ox}$  (a proxy for the measurable  $\Delta A_{480}$ ) are both sensitive to topology but have different dependencies, while the simulated results in Figure 7b illustrate that the coupling of these two measurements should enhance the ability to detect topology differences. The experimental results in Figure 7b are consistent with these simulations and illustrate the value of sensor fusion by spectroelectrochemical measurements.9

A second example of combining metrics is a discerning context (i.e., whether the film-coated electrode is in an oxidizing or reducing environment) that should be detected from current rectifications.<sup>38</sup> For instance, the schematic in Figure 7c illustrates that the addition of the yellow reducing node (i.e., ascorbate) is expected to enhance the flow of electrons through the Fc node to the electrode (i.e., increase Q<sup>ox</sup><sub>Fc</sub>) but inhibit the flow of electrons through the Ru<sup>3+</sup> node (i.e., decrease  $Q^{red}_{Ru}$ ). The simulation plot of  $Q^{red}_{Ru}$  vs  $Q^{ox}_{Fc}$  in Figure 7c shows that no rectification is expected for the threenode network (slope ≈ 1.0; black lines), while strong rectification (20-fold) is expected when the network is "perturbed" by the addition of the fourth reducing node. The experimental plot in Figure 7c is consistent with simulation. Overall, Figure 7 illustrates how the minimal model can be abstracted into readily measurable metrics to enable a data-driven analysis for interpreting measurements from more complex topological networks.

# CONCLUSIONS

Catechols are emerging as important molecular components in redox-based bioelectronics because they can engage biology in redox-based communication by exchanging electrons from various biological reductants and oxidants. 44,45,47 Importantly, electrofabrication allows electrodes to be coated with hydrogel films with thicknesses, catechol contents, and redox activities that can be tuned by fabrication conditions. 20,37 We envision

that catechol components can serve as "hubs", allowing catechol-coated electrodes to "plug into" biological redox networks to generate output signals that contain biologically relevant information.

Here, we used both time-series responses and phase-plane plots from dynamic analysis to characterize the underlying molecular phenomena of mediator diffusion and electron transfer. We found that the electron flow through the catechol film is networked, and the molecular switching of the catechol node is gated by the mediators and synchronized to the electron transfer at the electrode. We developed a minimal model that captures these experimental observations and abstracted output responses from steady dynamic analysis in terms of five metrics that were reliable (statistically significant correlations between simulation and experiment). We show that these metrics could be extrapolated to characterize output responses from less well-characterized electrode systems (i.e., ITO) and could detect perturbations associated with interactions of the catechol film with external redox nodes. We envision that these metrics and their combinations can be extended for multivariant machine learning to achieve the ultimate goal of "reconstructing" an unknown biological redox network. In summary, this study illustrates how a firstprinciples theory can be abstracted to yield system-level metrics that should enable a coupling of theory-guided and data-driven analysis for the emerging field of redox bioelectronics.

#### ASSOCIATED CONTENT

# **Supporting Information**

The Supporting Information is available free of charge at https://pubs.acs.org/doi/10.1021/acsaelm.2c00269.

Electrofabrication of catechol-based bioelectronics, evidence of negligible direct electron exchange of the catechol film and electrode, simulation model description, spatiotemporal variations in mediator concentrations, electrical charge phase-plane plot comparisons, spatiotemporal variations in catechol concentrations, dynamic analysis of electrical and molecular signals, ITO experimental charge detrending, theory-guided and datadriven analysis of network perturbations, and COMSOL model report (PDF)

# AUTHOR INFORMATION

## **Corresponding Author**

Gregory F. Payne — Institute for Bioscience and Biotechnology Research, University of Maryland, College Park, Maryland 20742, United States; Robert E. Fischell Institute for Biomedical Devices, University of Maryland, College Park, Maryland 20742, United States; ◎ orcid.org/0000-0001-6638-9459; Email: gpayne@umd.edu

## **Authors**

Zhiling Zhao — Institute for Bioscience and Biotechnology Research, University of Maryland, College Park, Maryland 20742, United States; Robert E. Fischell Institute for Biomedical Devices, University of Maryland, College Park, Maryland 20742, United States; orcid.org/0000-0003-0186-7215

Si Wu — College of Resources and Environmental Engineering, Hubei Key Laboratory for Efficient Utilization and Agglomeration of Metallurgic Mineral Resources, Wuhan

- University of Science and Technology, Wuhan 430081, China; orcid.org/0000-0001-6325-3951
- Eunkyoung Kim Institute for Bioscience and Biotechnology Research, University of Maryland, College Park, Maryland 20742, United States; Robert E. Fischell Institute for Biomedical Devices, University of Maryland, College Park, Maryland 20742, United States; orcid.org/0000-0003-2566-4041
- Chen-yu Chen Fischell Department of Bioengineering, University of Maryland, College Park, Maryland 20742, United States
- John R. Rzasa Robert E. Fischell Institute for Biomedical Devices, University of Maryland, College Park, Maryland 20742, United States; Fischell Department of Bioengineering, University of Maryland, College Park, Maryland 20742, United States
- Xiaowen Shi School of Resource and Environmental Science, Hubei International Scientific and Technological Cooperation Base of Sustainable Resource and Energy, Hubei Engineering Center of Natural Polymers-Based Medical Materials, Hubei Biomass-Resource Chemistry and Environmental Biotechnology Key Laboratory, Wuhan University, Wuhan 430079, China; orcid.org/0000-0001-8294-2920
- William E. Bentley Institute for Bioscience and Biotechnology Research and Fischell Department of Bioengineering, University of Maryland, College Park, Maryland 20742, United States; Robert E. Fischell Institute for Biomedical Devices, University of Maryland, College Park, Maryland 20742, United States; orcid.org/0000-0002-4855-7866

Complete contact information is available at: https://pubs.acs.org/10.1021/acsaelm.2c00269

## Notes

The authors declare no competing financial interest.

#### ACKNOWLEDGMENTS

This work was supported by the National Science Foundation (CBET #1932963), the Defense Threat Reduction Agency (HDTRA1-19-0021), and the Department of Energy, OBER, Lawrence Livermore National Laboratory SFA (under contracts DE-AC52-07NA27344 and LLNL-JRNL-827946).

#### REFERENCES

- (1) Parvez, S.; Long, M. J. C.; Poganik, J. R.; Aye, Y. Redox Signaling by Reactive Electrophiles and Oxidants. *Chem. Rev.* **2018**, *118*, 8798–8888.
- (2) Kim, E.; Li, J.; Kang, M.; Kelly, D. L.; Chen, S.; Napolitano, A.; Panzella, L.; Shi, X.; Yan, K.; Wu, S.; Shen, J.; Bentley, W. E.; Payne, G. F. Redox Is a Global Biodevice Information Processing Modality. *Proc. IEEE* **2019**, *107*, 1402–1424.
- (3) Liu, Y.; Li, J.; Tschirhart, T.; Terrell, J. L.; Kim, E.; Tsao, C. Y.; Kelly, D. L.; Bentley, W. E.; Payne, G. F. Connecting Biology to Electronics: Molecular Communication via Redox Modality. *Adv. Healthcare Mater.* **2017**, *6*, 1700789.
- (4) VanArsdale, E.; Pitzer, J.; Payne, G. F.; Bentley, W. E. Redox Electrochemistry to Interrogate and Control Biomolecular Communication. *Iscience* **2020**, 23, 101545.
- (5) Matthews, J. D.; Reedy, A. R.; Wu, H.; Hinrichs, B. H.; Darby, T. M.; Addis, C.; Robinson, B. S.; Go, Y. M.; Jones, D. P.; Jones, R. M.; Neish, A. S. Proteomic Analysis of Microbial Induced Redox-Dependent Intestinal Signaling. *Redox Biol.* **2019**, *20*, 526–532.
- (6) Timme-Laragy, A. R.; Hahn, M. E.; Hansen, J. M.; Rastogi, A.; Roy, M. A. Redox Stress and Signaling during Vertebrate Embryonic

- Development: Regulation and Responses. Semin. Cell Dev. Biol. 2018, 80, 17–28.
- (7) Cortese-Krott, M. M.; Koning, A.; Kuhnle, G. G. C.; Nagy, P.; Bianco, C. L.; Pasch, A.; Wink, D. A.; Fukuto, J. M.; Jackson, A. A.; Van Goor, H.; Olson, K. R.; Feelisch, M. The Reactive Species Interactome: Evolutionary Emergence, Biological Significance, and Opportunities for Redox Metabolomics and Personalized Medicine. *Antioxid. Redox Signaling* **2017**, *27*, 684–712.
- (8) Santolini, J.; Wootton, S. A.; Jackson, A. A.; Feelisch, M. The Redox Architecture of Physiological Function. *Curr. Opin. Physiol.* **2019**, *9*, 34–47.
- (9) Kang, M.; Kim, E.; Chen, S.; Bentley, W. E.; Kelly, D. L.; Payne, G. F. Signal Processing Approach to Probe Chemical Space for Discriminating Redox Signatures. *Biosens. Bioelectron.* **2018**, *112*, 127–135.
- (10) Kim, E.; Keskey, Z.; Kang, M.; Kitchen, C.; Bentley, W. E.; Chen, S.; Kelly, D. L.; Payne, G. F. Validation of Oxidative Stress Assay for Schizophrenia. *Schizophr. Res.* **2019**, 212, 126–133.
- (11) Kim, E.; Winkler, T. E.; Kitchen, C.; Kang, M.; Banis, G.; Bentley, W. E.; Kelly, D. L.; Ghodssi, R.; Payne, G. F. Redox Probing for Chemical Information of Oxidative Stress. *Anal. Chem.* **2017**, *89*, 1583–1592.
- (12) Zhao, Z.; Ozcan, E. E.; VanArsdale, E.; Li, J.; Kim, E.; Sandler, A. D.; Kelly, D. L.; Bentley, W. E.; Payne, G. F. Mediated Electrochemical Probing: A Systems-Level Tool for Redox Biology. *ACS Chem. Biol.* **2021**, *16*, 1099–1110.
- (13) Hu, K.; Liu, Y. L.; Oleinick, A.; Mirkin, M. V.; Huang, W. H.; Amatore, C. Nanoelectrodes for Intracellular Measurements of Reactive Oxygen and Nitrogen Species in Single Living Cells. *Curr. Opin. Electrochem.* **2020**, 22, 44–50.
- (14) Liu, Y. L.; Huang, W. H. Stretchable Electrochemical Sensors for Cell and Tissue Detection. *Angew. Chem., Int. Ed.* **2021**, *60*, 2757–2767.
- (15) Tschirhart, T.; Kim, E.; Mckay, R.; Ueda, H.; Wu, H. C.; Pottash, A. E.; Zargar, A.; Negrete, A.; Shiloach, J.; Payne, G. F.; Bentley, W. E. Electronic Control of Gene Expression and Cell Behaviour in Escherichia Coli through Redox Signalling. *Nat. Commun.* **2017**, *8*, 14030.
- (16) Gordonov, T.; Kim, E.; Cheng, Y.; Ben-Yoav, H.; Ghodssi, R.; Rubloff, G.; Yin, J. J.; Payne, G. F.; Bentley, W. E. Electronic Modulation of Biochemical Signal Generation. *Nat. Nanotechnol.* **2014**, *9*, 605–610.
- (17) Bhokisham, N.; VanArsdale, E.; Stephens, K. T.; Hauk, P.; Payne, G. F.; Bentley, W. E. A Redox-Based Electrogenetic CRISPR System to Connect with and Control Biological Information Networks. *Nat. Commun.* **2020**, *11*, 1–12.
- (18) Terrell, J. L.; Tschirhart, T.; Jahnke, J. P.; Stephens, K.; Liu, Y.; Dong, H.; Hurley, M. M.; Pozo, M.; McKay, R.; Tsao, C.-Y.; Wu, H. C.; Vora, G.; Payne, G. F.; Stratis-Cullum, D. N.; Bentley, W. E. Bioelectronic Control of a Microbial Community Using Surface-Assembled Electrogenetic Cells to Route Signals. *Nat. Nanotechnol.* **2021**, *16*, 688–697.
- (19) Motabar, D.; Li, J.; Payne, G. F.; Bentley, W. E. Mediated Electrochemistry for Redox-Based Biological Targeting: Entangling Sensing and Actuation for Maximizing Information Transfer. *Curr. Opin. Biotechnol.* **2021**, *71*, 137–144.
- (20) Wu, S.; Kim, E.; Chen, C.; Li, J.; VanArsdale, E.; Grieco, C.; Kohler, B.; Bentley, W. E.; Shi, X.; Payne, G. F. Catechol-Based Molecular Memory Film for Redox Linked Bioelectronics. *Adv. Electron. Mater.* **2020**, *6*, 2000452.
- (21) Kim, E.; Zhao, Z.; Rzasa, J. R.; Glassman, M.; Bentley, W. E.; Chen, S.; Kelly, D. L.; Payne, G. F. Association of Acute Psychosocial Stress with Oxidative Stress: Evidence from Serum Analysis. *Redox Biol.* **2021**, *47*, 102138.
- (22) Callaway, C. P.; Liu, A. L.; Venkatesh, R.; Zheng, Y.; Lee, M.; Meredith, J. C.; Grover, M.; Risko, C.; Reichmanis, E. The Solution Is the Solution: Data-Driven Elucidation of Solution-to-Device Feature Transfer for π-Conjugated Polymer Semiconductors. *ACS Appl. Mater. Interfaces* **2022**, *14*, 3613–3620.

- (23) Alber, M.; Buganza Tepole, A.; Cannon, W. R.; De, S.; Dura-Bernal, S.; Garikipati, K.; Karniadakis, G.; Lytton, W. W.; Perdikaris, P.; Petzold, L.; Kuhl, E. Integrating Machine Learning and Multiscale Modeling: Perspectives, Challenges, and Opportunities in the Biological, Biomedical, and Behavioral Sciences. *npj Digit. Med.* **2019**, *2*, 1–11.
- (24) Kwon, I. S.; Kim, Y. J.; Klosterman, L.; Forssell, M.; Fedder, G. K.; Bettinger, C. J. In Vitro Electrochemical Characterization of Polydopamine Melanin as a Tissue Stimulating Electrode Material. *J. Mater. Chem. B* **2016**, *4*, 3031–3036.
- (25) Bettinger, C. J. Advances in Materials and Structures for Ingestible Electromechanical Medical Devices. *Angew. Chem., Int. Ed.* **2018**, *57*, 16946–16958.
- (26) Zhou, X.; McCallum, N. C.; Hu, Z.; Cao, W.; Gnanasekaran, K.; Feng, Y.; Stoddart, J. F.; Wang, Z.; Gianneschi, N. C. Artificial Allomelanin Nanoparticles. *ACS Nano* **2019**, *13*, 10980–10990.
- (27) Cao, W.; Mantanona, A. J.; Mao, H.; McCallum, N. C.; Jiao, Y.; Battistella, C.; Caponetti, V.; Zang, N.; Thompson, M. P.; Montalti, M.; Stoddart, J. F.; Wasielewski, M. R.; Rinehart, J. D.; Gianneschi, N. C. Radical-Enriched Artificial Melanin. *Chem. Mater.* **2020**, *32*, 5759–5767
- (28) Lee, H. A.; Park, E.; Lee, H. Polydopamine and Its Derivative Surface Chemistry in Material Science: A Focused Review for Studies at KAIST. *Adv. Mater.* **2020**, *32*, 1907505.
- (29) Wu, S.; Kim, E.; Li, J.; Bentley, W. E.; Shi, X.-W.; Payne, G. F. Catechol-Based Capacitor for Redox-Linked Bioelectronics. *ACS Appl. Electron. Mater.* **2019**, *1*, 1337–1347.
- (30) Jin, Z.; Yang, L.; Shi, S.; Wang, T.; Duan, G.; Liu, X.; Li, Y. Flexible Polydopamine Bioelectronics. *Adv. Funct. Mater.* **2021**, *31*, 2103391.
- (31) Yang, P.; Zhu, F.; Zhang, Z.; Cheng, Y.; Wang, Z.; Li, Y. Stimuli-Responsive Polydopamine-Based Smart Materials. *Chem. Soc. Rev.* **2021**, *50*, 8319–8343.
- (32) Wu, L. Q.; Ghodssi, R.; Elabd, Y. A.; Payne, G. F. Biomimetic Pattern Transfer. *Adv. Funct. Mater.* **2005**, *15*, 189–195.
- (33) Wu, L.-Q.; McDermott, M. K.; Zhu, C.; Ghodssi, R.; Payne, G. F. Mimicking Biological Phenol Reaction Cascades to Confer Mechanical Function. *Adv. Funct. Mater.* **2006**, *16*, 1967–1974.
- (34) Cheng, Y.; Luo, X.; Betz, J.; Buckhout-White, S.; Bekdash, O.; Payne, G. F.; Bentley, W. E.; Rubloff, G. W. In Situ Quantitative Visualization and Characterization of Chitosan Electrodeposition with Paired Sidewall Electrodes. *Soft Matter* **2010**, *6*, 3177–3183.
- (35) Zangmeister, R. A.; Park, J. J.; Rubloff, G. W.; Tarlov, M. J. Electrochemical Study of Chitosan Films Deposited from Solution at Reducing Potentials. *Electrochim. Acta* **2006**, *51*, 5324–5333.
- (36) Kim, E.; Leverage, W. T.; Liu, Y.; White, I. M.; Bentley, W. E.; Payne, G. F. Redox-Capacitor to Connect Electrochemistry to Redox-Biology. *Analyst* **2014**, *139*, 32–43.
- (37) Kim, E.; Liu, Y.; Shi, X. W.; Yang, X.; Bentley, W. E.; Payne, G. F. Biomimetic Approach to Confer Redox Activity to Thin Chitosan Films. *Adv. Funct. Mater.* **2010**, *20*, 2683–2694.
- (38) Kim, E.; Gordonov, T.; Liu, Y.; Bentley, W. E.; Payne, G. F. Reverse Engineering to Suggest Biologically Relevant Redox Activities of Phenolic Materials. *ACS Chem. Biol.* **2013**, *8*, 716–724.
- (39) Liu, Y.; Kim, E.; Lee, M. E.; Zhang, B.; Elabd, Y. A.; Wang, Q.; White, I. M.; Bentley, W. E.; Payne, G. F. Enzymatic Writing to Soft Films: Potential to Filter, Store, and Analyze Biologically Relevant Chemical Information. *Adv. Funct. Mater.* **2014**, *24*, 480–491.
- (40) Schmidt, I.; Gad, A.; Scholz, G.; Boht, H.; Martens, M.; Schilling, M.; Wasisto, H. S.; Waag, A.; Schröder, U. Gold-Modified Indium Tin Oxide as a Transparent Window in Optoelectronic Diagnostics of Electrochemically Active Biofilms. *Biosens. Bioelectron.* 2017, 94, 74–80.
- (41) Fu, Y.; Zhang, J.; Wang, Y.; Li, J.; Bao, J.; Xu, X.; Zhang, C.; Li, Y.; Wu, H.; Gu, Z. Reduced Polydopamine Nanoparticles Incorporated Oxidized Dextran/Chitosan Hybrid Hydrogels with Enhanced Antioxidative and Antibacterial Properties for Accelerated Wound Healing. *Carbohydr. Polym.* **2021**, 257, 117598.

- (42) Ding, T.; Wang, Z.; Xia, D.; Zhu, J.; Huang, J.; Xing, Y.; Wang, S.; Chen, Y.; Zhang, J.; Cai, K. Long-Lasting Reactive Oxygen Species Generation by Porous Redox Mediator-Potentiated Nanoreactor for Effective Tumor Therapy. *Adv. Funct. Mater.* **2021**, *31*, 2008573.
- (43) Xie, X.; Wang, Z.; Zhou, M.; Xing, Y.; Chen, Y.; Huang, J.; Cai, K.; Zhang, J. Redox Host–Guest Nanosensors Installed with DNA Gatekeepers for Immobilization-Free and Ratiometric Electrochemical Detection of MiRNA. *Small Methods* **2021**, *5*, 2101072.
- (44) Wu, S.; Zhao, Z.; Rzasa, J. R.; Kim, E.; Li, J.; VanArsdale, E.; Bentley, W. E.; Shi, X.; Payne, G. F. Hydrogel Patterning with Catechol Enables Networked Electron Flow. *Adv. Funct. Mater.* **2020**, *31*, 2007709.
- (45) Kim, E.; Liu, Y.; Bentley, W. E.; Payne, G. F. Redox Capacitor to Establish Bio-Device Redox-Connectivity. *Adv. Funct. Mater.* **2012**, 22, 1409–1416.
- (46) Li, Y.; Liu, Y.; Kim, E.; Song, Y.; Tsao, C. Y.; Teng, Z.; Gao, T.; Mei, L.; Bentley, W. E.; Payne, G. F.; Wang, Q. Electrodeposition of a Magnetic and Redox-Active Chitosan Film for Capturing and Sensing Metabolic Active Bacteria. *Carbohydr. Polym.* **2018**, *195*, 505–514.
- (47) Kim, E.; Gordonov, T.; Bentley, W. E.; Payne, G. F. Amplified and in Situ Detection of Redox-Active Metabolite Using a Biobased Redox Capacitor. *Anal. Chem.* **2013**, *85*, 2102–2108.
- (48) Du, J.; Cullen, J. J.; Buettner, G. R. Ascorbic Acid: Chemistry, Biology and the Treatment of Cancer. *Biochim. Biophys. Acta Rev. Cancer* **2012**, *1826*, 443–457.
- (49) Paciolla, C.; Fortunato, S.; Dipierro, N.; Paradiso, A.; De Leonardis, D.; Mastropasqua, L.; de Pinto, M. C. Vitamin C in Plants: From Functions to Biofortification. *Antioxidants* **2019**, *8*, 519.
- (50) Hughes, D. E. Irreversible Reaction Kinetics of the Aerobic Oxidation of Ascorbic Acid. *Anal. Chem.* **1985**, *57*, 555–558.
- (51) Raman, K.; Raman, K. An Introduction to Computational Systems Biology: Systems-Level Modelling of Cellular Networks; CRC Press, 2021, 115.
- (52) Liu, A. L.; Venkatesh, R.; McBride, M.; Reichmanis, E.; Meredith, J. C.; Grover, M. A. Small Data Machine Learning: Classification and Prediction of Poly (Ethylene Terephthalate) Stabilizers Using Molecular Descriptors. ACS Appl. Polym. Mater. 2020, 2, 5592–5601.
- (53) Venkatesh, R.; Zheng, Y.; Viersen, C.; Liu, A.; Silva, C.; Grover, M.; Reichmanis, E. Data Science Guided Experiments Identify Conjugated Polymer Solution Concentration as a Key Parameter in Device Performance. ACS Mater. Lett. 2021, 3, 1321–1327.